Graphene Oxide Exoskeleton to Produce SelfExtinguishing, Nonignitable, and Flame Resistant Flexible Foams: A Mechanically Tough Alternative to Inorganic Aerogels

ADVANCED MATERIALS INTERFACES

www.advmatinterfaces.de

Graphene Oxide Exoskeleton to Produce Self-Extinguishing, Nonignitable, and Flame Resistant Flexible Foams: A Mechanically Tough Alternative to Inorganic Aerogels

*Federico Carosio, Lorenza Maddalena, Julio Gomez, Guido Saracco, and Alberto Fina**

The potential safety hazard associated to commonly used flame retardant chemicals generates a strong demand for new, sustainable, and high performing solutions to reduce the fire threats of widespread polymer foams. In this work, the production of self-extinguishing, nonignitable, and flame resistant flexible polyurethane foams by means of simple layer-by-layer assembly of graphene oxide nanoplatelets is reported. The process builds a protective exoskeleton that completely wraps the complex 3D structure of the foam and is capable of stopping flame spread in flammability tests and preventing ignition when exposed to heat fluxes typical of developing fires. In addition, treated foams are found able to withstand the penetration of a flame torch, successfully protecting the unexposed side from thermal decomposition for more than 6 min. The outstanding temperature gradient greater than 500 °C cm^{-1} achieved through the foam thickness makes the performances of these foams comparable to those of a silica aerogel, while maintaining excellent flexibility and toughness. The results reported in this paper represent a tremendous opportunity for the production of a novel class of organic and flexible foams, capable of ensuring unprecedented fire safety properties while relying on an easy, green, and straightforward approach to material design.

1. Introduction

Nowadays, polymer foams are widely employed in a various applications such as packaging, furniture cushioning and insulator materials. This is related to the unique set of advantageous properties associated to this class of materials. Indeed, their low density, very low acoustic and/or heat transfer, make them optimal solutions for applications in civil, residential, and industrial buildings. Furthermore, flexible and soft foams provide comfort when used for furniture or seats cushioning employed in houses or transportations. Unfortunately, their inherent organic nature poses severe risks of fire as they can ignite very easily and burn at a high rate, due to their low density, which statistically makes polymer foams one of the first items to be ignited during a fire.[1] For this reason, flame retardant (FR) chemicals are normally employed to ensure the safety of humans in public buildings, industries and transports.[2] However, in recent years the increasing societal awareness for potential toxicological and environmental risks associated to the use of some of the most widely used and performing FR chemicals has led to the attempt of partial substitution with safer products and sometimes even to their reduction or removal from polymer formulations.[3,4] This inevitably increased the risk of fire events that can be extremely devastating as demonstrated by recent events.[5] For the mentioned reasons, researchers have been working on the development of novel foams characterized by improved flame retardant properties using nanotechnology by means of green routes. To this aim, freeze-casting techniques have been widely exploited for the construction of rigid low density foams characterized by either random or oriented structures.[6] The produced foams normally contain an organic matrix such as alginates or nanocellulose and a large volume fraction of inorganic nanoparticles such as layered double hydroxide, sodium montmorillonite, kaolin, and sepiolite.[7–10] This composition and unique structure normally allows self-extinguishing properties and very low heat release rates during combustion making them superior to commercially available rigid foams. However, the use of ice-templating techniques is rather limiting for what concerns the processing time and foam size, eventually representing a big constrain to possible industrial applications. Another approach is represented by the surface nanostructuration of foams by means of the layer-by-layer (LbL) deposition.[11–13] This technique allows to target open cell foams, including the most common and highly flammable polyurethane (PU) foams, ubiquitous

Dr. F. Carosio, L. Maddalena, Prof. G. Saracco, Prof. A. Fina
Dipartimento di Scienza Applicata e Tecnologia
Politecnico di Torino
Alessandria Campus, Viale Teresa Michel 5, 15121 Alessandria, Italy
E-mail: alberto.fina@polito.it

J. Gomez
Avanzare Innovacion Tecnologica S.L
Avda. Lenticares 4-6
Poligono Industrial Lentiscares
26370 Navarrete (la Rioja), Spain

The ORCID identification number(s) for the author(s) of this article can be found under https://doi.org/10.1002/admi.201801288.

DOI: 10.1002/admi.201801288

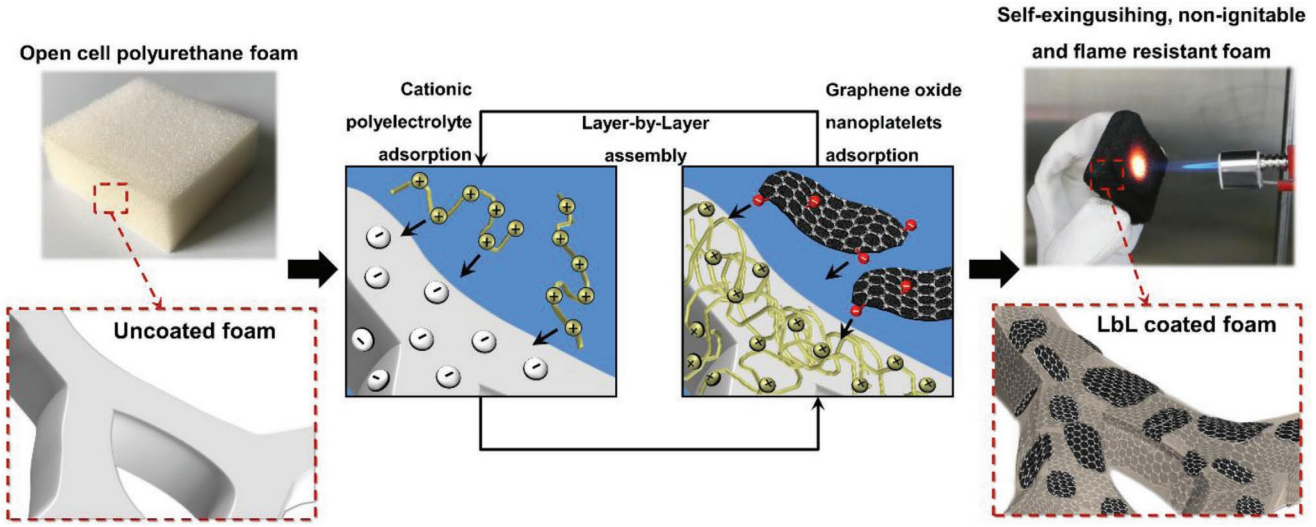

Figure 1. Schematic representation of the deposited LbL assembly. PU foams are alternatively dipped in cationic polyelectrolyte solution and negative graphene oxide nanoplatelets suspension. Each cycle deposits a bi-layer (BL), the process is repeated in order to deposit 3BL and 6BL.

in buildings and transportation.[14] Indeed, the LbL approach offers a versatile and straightforward tool for the assembly of nanostructured coatings with precise composition and through thickness preferential orientation thus achieving a sort of exoskeleton on the complex 3D structure of the foam.[15,16] The selected coating constituents are assembled on the surface of a substrate by sequential adsorption from aqueous based solutions/suspension in template assisted assembly fashion.[17] Beside foams, this technique has been also used to produce fire retardant fabrics and thin films demonstrating a direct dependence between the achieved properties and the assembly conditions such as pH, ionic strength and molecular weight.[18–22] As far as foams are concerned, it has been demonstrated that the incorporation of nanoparticles within the assembly is an almost mandatory condition in order to achieve the best fire retardant properties.[18] Most developed LbL systems achieve substantial reductions in burning rates whereas only few can grant, at the cost of a high number of deposition steps, the suppression of flame spread.[23,24] This limits the applicability and potential of LbL treated PU foams and suggests that a scientific breakthrough is needed to unveil the true potentialities of LbL in producing flexible foams well beyond the state of the art. Thus, in contrast with previously reported research, in the present paper we report the use of LbL assembly for the production of PU foams characterized by never reported before flame retardant and fire resistant properties. To this aim highly oriented nanostructured films encompassing graphene oxide nanoplatelets (GO) have been assembled on the 3D internal structure of PU foams producing a fire proofing exoskeleton as schematically depicted in **Figure 1**.

Graphene related materials are known to be promising building blocks for the construction of advanced materials.[25–29] In particular GO has been successfully exploited in water based processes for the production of flame retardant films and foams.[30–32] In this work, we exploit the electrostatic interaction occurring between negatively charged GO nanoplatelets and a synthetic positively charged strong polyelectrolyte, the poly(diallyldimethylammonium chloride) (PDAC). The LbL assembly has been first evaluated revealing a linear growth that is further improved in terms of thickness per deposited layer by the inclusion of a phosphate salt. This PDAC/GO system can conformally coat every surface of the PU foam resulting in a protecting exoskeleton comprising highly oriented GO nanoplatelets. Only 3 BL assembled in modified ionic strength conditions can suppress flame spread in flammability test and completely prevent foam ignition during cone calorimetry tests. Treated foams are also found able to withstand the penetration of a flame torch resulting in fire resistance performances similar to those achievable with a completely inorganic silica aerogel. This paper represents a tremendous opportunity for the development of fire safe flexible foams.

2. Results and Discussion

2.1. Coating Growth by Fourier Transformed-Infrared (FT-IR) Spectroscopy

First of all, the spectra of neat components were evaluated and are reported in Figure S2 (Supporting Information) while Table S2 (Supporting Information) collects the detailed list of signals. PDAC shows the main characteristics bands associated to C—H bonds in CH_2 (3020 and 1472 cm^{-1}) and CH_3 (2944 and 2871 cm^{-1}) and N—C bonds (1145 cm^{-1}).[33] Signals ascribed to adsorbed water are recognizable as well at 1640 cm^{-1} (OH bending) and the broad band centered at 3400 (O—H stretching). Neat GO spectrum evidences the presence of oxidized groups with bands at 1725, 1627, and 1054 cm^{-1} that can be related to COOH, COO^-, and C—O, respectively.[34] Hydroxyl groups are also visible in the range between 3400 and 3000 cm^{-1}. On the other hand, neat ammonium phosphate dibasic (APD) yields signals ascribed to $N—H^+$ and N—H vibrations in NH_4^+ at 3300–3030 and 1410 cm^{-1}, respectively as well as to phosphate groups P=O, PO_3^{2-}, P—O at 1260, 1080, and 900 cm^{-1}, respectively.[35]

The LbL growth of PDAC/GO system under 0 and 0.5M ionic strength conditions was monitored by FT-IR spectroscopy.

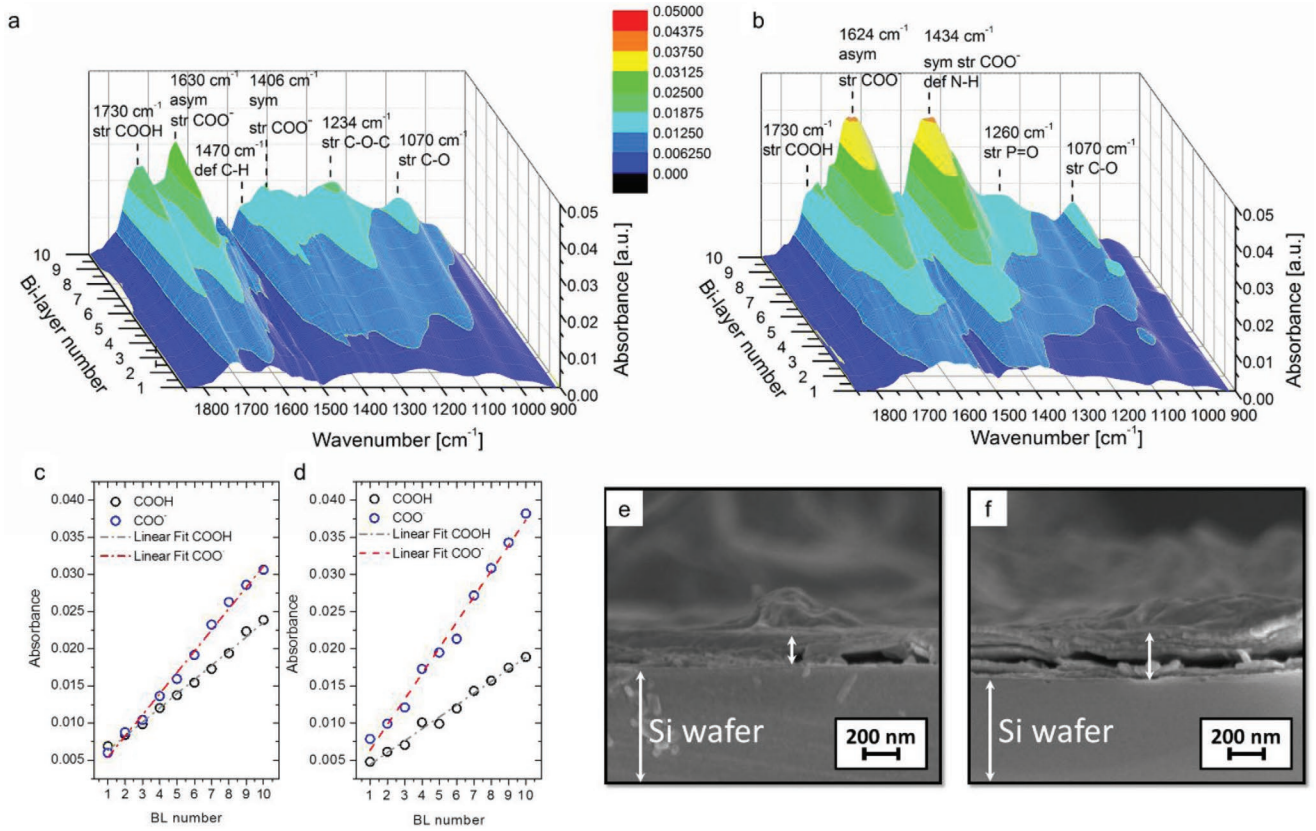

Figure 2. Characterization of the build-up of PDAC/GO at 0 a,c,e) and 0.5M b,d,f) APD on model Si substrate: a,b) FT-IR spectra in the 1850–900 cm^{-1} region during LbL growth; c,d) evolution of the signals ascribed to COOH and COO^- as function of bilayer number and e,f) FE-SEM micrographs of 10 BL cross-section on Si wafer.

Figure 2 reports the resulting 3D projection of restricted IR region, the intensity of the peaks ascribed to COOH and COO^- plotted as a function of BL number and the cross section images of the 10BL coating imaged by FESEM.

When PDAC and GO are LbL assembled together their characteristic IR peaks add up in spectra that grows in intensity as the number of deposited bilayers is increased thus confirming the occurrence of a LbL growth (Figure 2a). The most intense peaks are ascribed to GO indicating its greater abundance with respect to PDAC in the assembly. By plotting the intensity of COOH and COO^- signals as a function of BL number it is possible to devise a linear growth regime for the assembly. The incorporation of APD in the GO suspension is responsible for a change in the IR signals observed. Indeed, as reported in Figure 2b, GO signals ascribed to COO^- groups strongly increase in intensity while the COOH peak is considerably reduced to a shoulder of the main peak centered at 1624 cm^{-1}. This is explained by the alkaline nature of APD, that promotes the conversion of GO carboxyl groups to ammonium carboxylates.[36,37] In addition, as already reported in LbL systems assembled at modified ionic strength,[38] the presence of N—H and P=O signals (1434 and 1260 cm^{-1}, respectively) suggests that phosphates and ammonium ions remain incorporated in the assembly as counterions for PDAC and GO, respectively. Despite the change in the COOH/COO^- ratio, a linear growth regime was obtained for both formulations, as demonstrated by intensity versus BL number plots in Figure 2d. Nevertheless, the presence of APD in the GO suspension allows for the deposition of a thicker (≈ +70%) coating as pointed out by cross-section FESEM images of Si wafers coated by 10 BL assembled at unmodified and modified ionic strength (Figure 2e,f, respectively). The layered structure of the coating comprising GO nanoplatelets held together by PDAC is apparent for both assemblies. From the above mentioned observations it is therefore proved that the presence of APD promotes the deposition of thicker coatings. This is achieved, in accordance with previously reported literature, on one hand by allowing the deposition of stacked GO nanoplatelets due to the change in ionic strength and on the other hand by incorporating the salt within the assembled structure.[22,38]

2.2. Morphology of the Coating on PU Foams

Both the assemblies studied before have been deposited on neat PU foams aiming to a total of 3 and 6 BL. The resulting changes in surface morphology have been imaged by FESEM. **Figure 3** reports micrographs of modified foams in comparison with the pristine one.

Neat PU displays a typical open cell structure with cell walls characterized by an even and smooth surface (Figure 3a). The LbL deposition completely changes the micrometer-scale morphology of the foam without blocking the pores thus

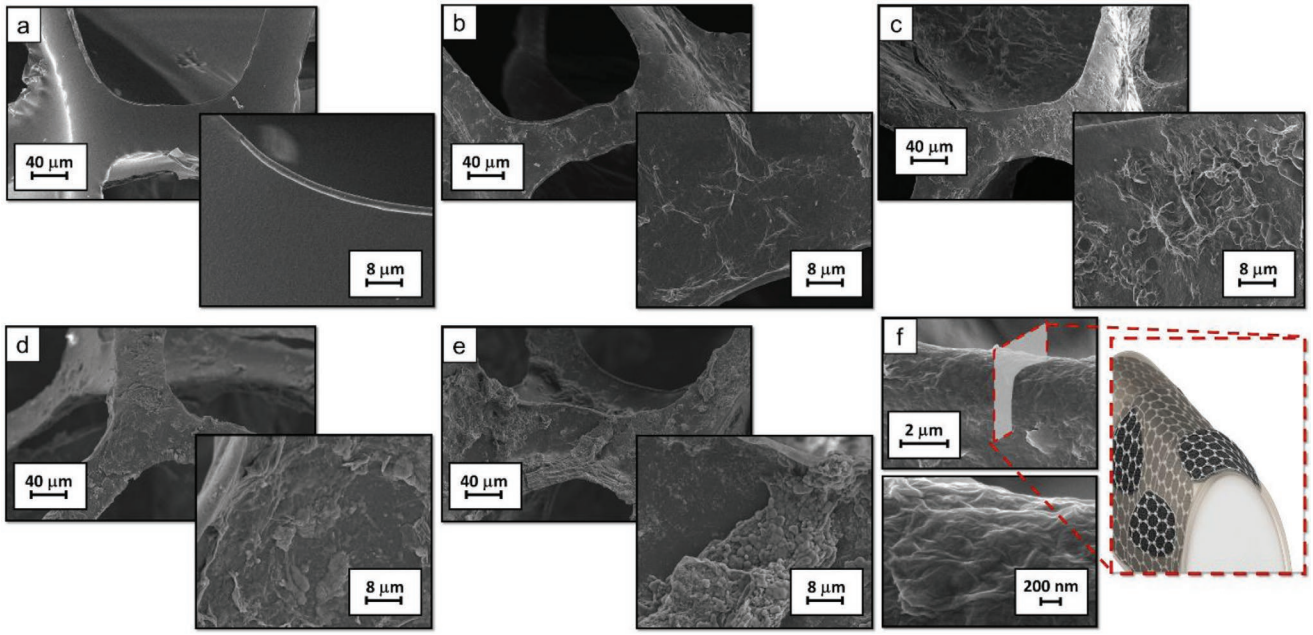

Figure 3. SEM micrograph of untreated and LbL treated PU foam: a) neat PU, b) 3BL, c) 3 BL 0.5M, d) 6 BL, e) 6 BL 0.5M, and f) detail and schematization of coating on the foam edge.

keeping unaltered its macroscopic nature as observable from low magnification micrographs in Figure S3 (Supporting Information). Indeed, the LbL assembled PDAC/GO homogenously coat every surface available resulting in a conformal coating that extends through the entire thickness of the foam (Figure 3b–e). This occurs after 3 BL and can be ascribed to the initial surface activation step and the high aspect ratio of the employed GO. The thickness of the deposited coating increases by increasing the number of deposited BL and its maximized by the presence of APD in the GO suspension in agreement with what observed on model Si surfaces (compare Figure 3b with c and Figure 3d with e). This suggests a good stability of the water swelled deposited layers that can survive the mechanical deformation imparted to the foam during the deposition process and yield a steady coating build up in agreement with what already reported in the literature.[39] Furthermore, a few crystals can be observed on top of the coating (Figure 3c,e), likely related to the excess of salt in the solution, as suggested by the presence of phosphorous in their elemental analysis. Elemental analyses further prove that phosphates are also found embedded within the coating (Figure S4, Supporting Information). In addition, it is worth noting the high flexibility of employed GO nanoplatelets that are able to bend over submicronic radii in order to follow the PU complex geometry as imaged and schematized in Figure 3f.

2.3. Flame Retardancy Characterization

The flame retardant properties of prepared foams have been thoroughly evaluated by means of flammability and cone calorimetry tests. These two tests provide a complete set of information concerning the contribution of a material in either initiating a fire (exposure to a small flame, flammability) or contributing to its growth (exposure to a heat flux, cone calorimetry). **Figure 4** summarizes collected data while Tables S3 and S4 (Supporting Information) report numerical parameters registered during the tests.

The application of a small flame to unmodified PU foam can easily set it on fire. The flames rapidly propagate to the entire sample causing the formation of incandescent/flaming droplets of molten polymer that fall underneath the sample and ignite the dry cotton (Figure 4a). This phenomenon is known as melt-dripping and it is a typical fire threat of synthetic polymers as the flaming droplets can easily spread the fire to other ignitable items, thus detrimentally contributing to fire growth. The presence of the LbL coatings completely changes this behavior. Indeed, 3 and 6 BL coatings assembled at unmodified ionic strength are capable of suppressing the melt dripping behavior and completely maintain the original shape of the foam. The flame spread to the entire length of the sample but are confined only on the surface of the sample as evidenced by cutting the cross section of the samples at the end of the tests. This is also confirmed by the high residues obtained (60 and 78 wt% for 3 and 6 BL, respectively) point out that the flame self-extinguishes before being able to completely decompose and volatilize the underlying PU. On the other hand, coatings assembled at modified ionic strength are capable of not only suppressing the melt dripping, but also completely preventing flame spreading by self-extinguishing the flame within 5–10 s after flame application. Subsequent and prolonged flame applications cannot ignite the sample again. For this reason the final residues are as high as 98–99%. Cone calorimetry tests have been performed to evaluate the reaction to the exposure to a heat flux typical of fires in early stages (35 kW m^{-2}). The exposure to such heat flux quickly triggers the PU foam decomposition processes with the release of highly flammable volatiles gases that lead to sample ignition and flaming combustion measured as heat release rate versus time plot (Figure 4c).

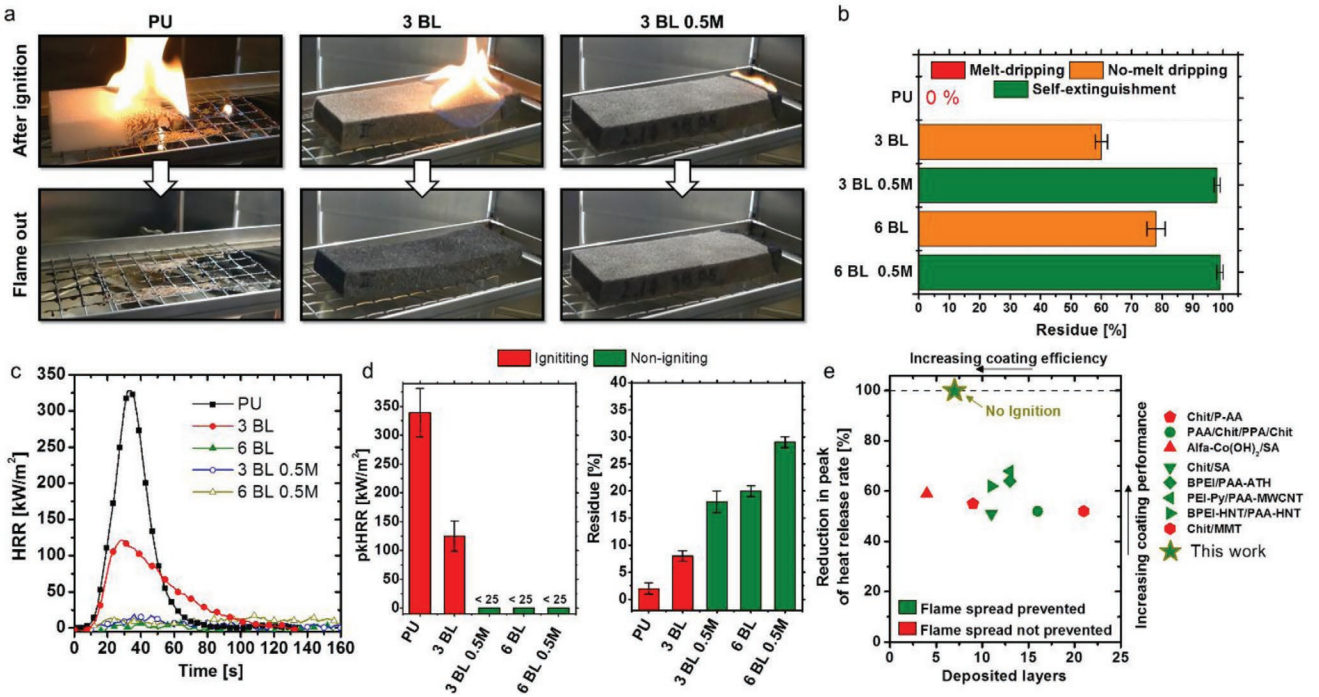

Figure 4. Flame retardant characterization of untreated and LbL treated foams: a) snapshots from flammability tests, b) average residues after flammability tests, c) heat release rate versus time plots, d) average peak of heat release rate and final residue, and e) flame retardant performance comparison with previously reported materials.

The PU foam quick ignition followed by its structural collapse creates a pool of low viscosity liquid with a steeply increase in the heat release rate that reaches its maximum value (pkHRR = 322 kW m^{-2}). The foam is almost completely consumed by combustion leaving a residue accounting for 1–2% of the original mass and related to minor charring and/or the presence of solid additives in the PU (Figure 4d). The deposition of 3 BL at unmodified ionic strength can prevent the foam structural collapse after ignition and considerably reduce the pkHRR values by 60%. Unexpectedly, all the other samples showed no ignition at all during the whole test. Clearly, the exposure to 35 kW m^{-2} still triggers the PU decomposition with release of flammable volatiles; however, the concentration of such volatiles remains below the lower flammability limit and thus ignition cannot occur. Such impressive behavior is totally unexpected for organic materials and it has been never reported for PU foams thus representing a dramatic increase in the fire safety of prepared foams. All nonigniting foams yielded a coherent residue that maintained the original dimensions of the starting sample also displaying a certain degree of mechanical resistance by maintaining shape and structural integrity when compressed by 13 g cm^{-2} (Figure S5a–f, Supporting Information). In order to better highlight the importance of the achieved results, a comparison with previously reported LbL coating comprising inorganic nanoplatelets, natural polysaccharides or carbon nanotubes for foam flame retardancy is presented in Figure 4e.[23,24,40–45] The reduction in heat release rate peak as function of deposited layer number is evaluated; the ability to self-extinguish the flame and prevent its spread to the entire surface of the sample during flammability tests is also accounted for (red or green symbols). What is apparent is that, although a substantial reduction (60–70%) of pkHRR can be easily achieved, a minimum number of 10 deposited layers are needed to achieve self-extinguishing behavior during flammability tests. Conversely, in the present work we demonstrate how 3BL (7 deposited layers) can self-extinguish the flame in flammability tests and prevent ignition during cone calorimetry tests: a unique set of properties never reported before.

2.4. Post Combustion Residue Analysis

All treated foams yielded a self-supported residue at the end of cone calorimetry testing (Figure S5, Supporting Information). Their microstructure and chemical composition have been investigated by means of SEM, Raman and attenuated total reflectance (ATR)-IR spectroscopy in order to investigate the evolution of the PDAC/GO assembly during combustion. SEM images and Raman spectra are collected in **Figure 5** while Figures S6 and S7 (Supporting Information) collect low magnification SEM micrographs and ATR-IR spectra, respectively.

From an overall point of view, the morphology of the residue closely resembles the one of the uncombusted samples. The presence of a compact hollow structure comprising GO nanoplatelets is apparent. This exoskeleton, similarly to the original LbL coating, wraps the entire 3D structure of the original PU foam that was volatilized during the testing. Its thickness and structural integrity increase by increasing the number of deposited BL and by moving from unmodified to modified ionic strength. The 3 BL that ignited during the test shows the formation of small cracks in the above mentioned structure. Such cracks might have compromised the integrity of

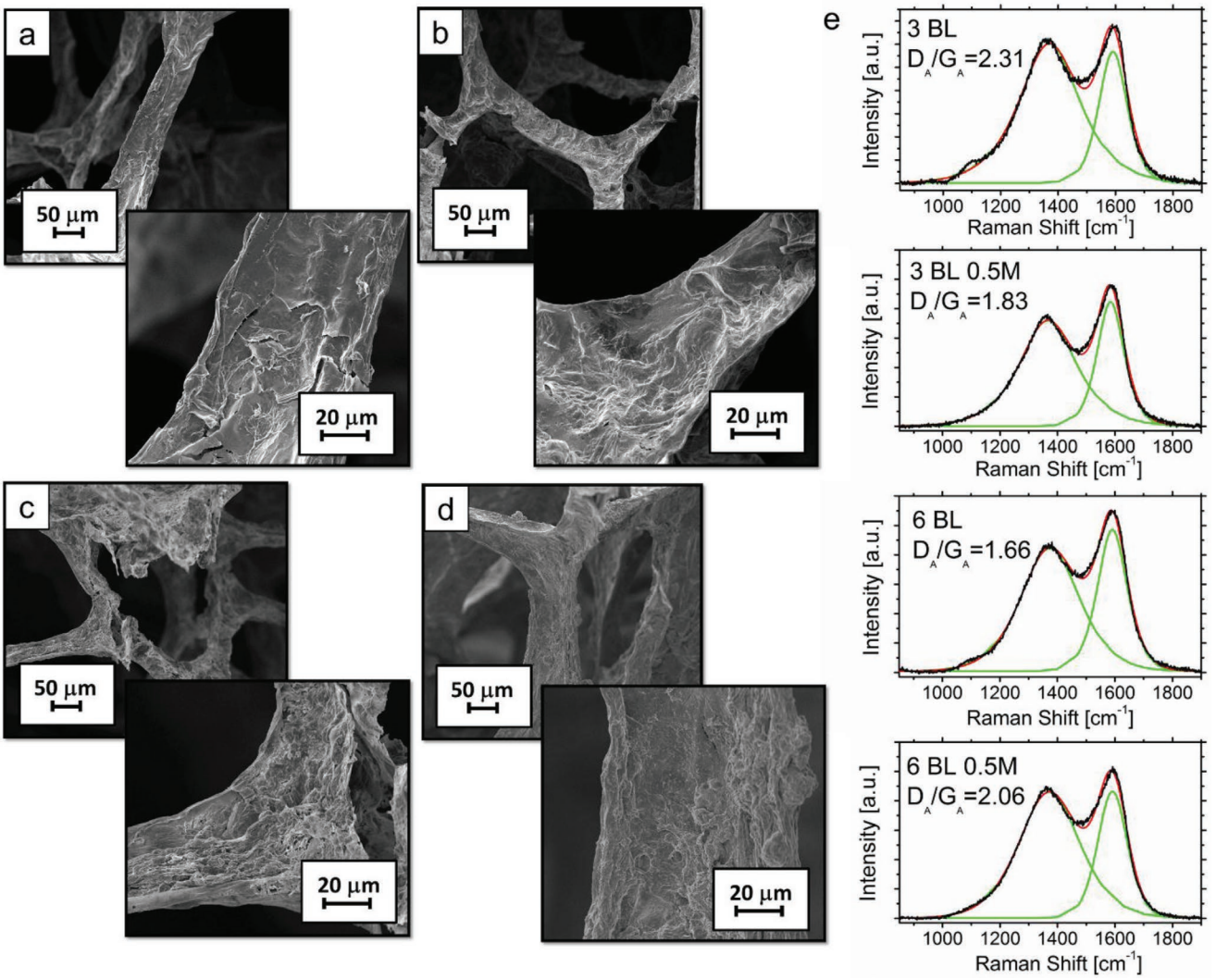

Figure 5. Post combustion residue analysis. SEM micrographs of: a) 3 BL, b) 3 BL 0.5M, c) 6 BL, and d) 6BL 0.5M). Raman spectra e) of LbL treated PU foam residues after cone calorimetry.

the coating and thus reduced its flame retardant efficiency. On the other hand, the residues from nonigniting samples appear undamaged indicating that an increase in coating thickness is beneficial in terms of flame retardant performances. Raman spectroscopy performed on the residues reveal the presence of two characteristic signals, known as G and D bands naturally present in the original GO (Figure S1, Supporting Information), clearly visible at 1590 and 1350 cm^{-1}.[46] In addition, interbands D*, D″, and D′ are also responsible of the width and intensity of D and G bands.[47] The evaluation of the ratio between the area underneath the G and D bands provides useful information about the quality of the carbon structure. Indeed, as reported in the literature, the D band is normally associated to number, type and distance between defects and crystallinity of sheets and is employed to evaluate the quality of graphene-based material.[48] The starting GO had a D_A/G_A ratio of 1.08 that is increased for all the samples after combustion tests due to char formation reactions of both PU and PDAC (see values in Figure 5e) accordingly with residue values reported in Table S4 (Supporting Information). The occurrence of ignition and the presence of phosphate salts (a well-known charring agent)[49] appear to provide competing char forming effects on PU and PDAC eventually resulting in different D_A/G_A ratios. Indeed, 3 and 6 BL at unmodified ionic strength achieve the highest and lowest ratios, respectively whereas samples at modified ionic strength fall within these values. ATR spectroscopy confirms the presence of conjugated C=C bonds (1570 cm^{-1}) as well as C=O (1730 cm^{-1}) and P−O−C (1085 cm^{-1}) bonds, these latter only visible for samples prepared at modified ionic strength (Figure S7, Supporting Information).[35]

The reported data clearly demonstrates the construction, upon temperature increase, of a stable structure comprising GO embedded in a charred matrix. The formation of this latter is promoted by the presence of phosphates embedded within the LbL coating. The resulting structure acts as an efficient barrier to heat and volatiles while also mechanically sustaining the PU foam and preventing its collapsing thus resulting in a tremendous FR effect.

2.5. Flame Penetration Tests

Self-extinguishing and nonigniting samples have been selected for flame penetration tests. This test evaluates the resistance of the foam to the penetration of a flame focused on one side of the sample and reproduces a larger scale test normally employed to evaluate the fire resistance of composites containing a relatively high fraction of inorganic filler. During the performed small scale tests a square sample is positioned in a ceramic frame; one side is then exposed to a butane flame torch positioned at 50 mm which result in a surface temperature of about 950 °C. Two thermocouples monitor the temperatures on both the exposed and unexposed side. A schematization of this test layout is reported in **Figure 6** along with temperature profiles and snapshots taken during the tests for 6 BL at modified ionic strength in comparison with a silica aerogel. Figure S8 (Supporting Information) collects snapshots of untreated PU and 3 BL 0.5M as well as the temperature profiles for this latter.

The unmodified PU foam is immediately destroyed by the flame torch and the tests only lasts for few seconds (Figure S8, Supporting Information). Conversely, the 3 BL 0.5M samples can withstand the penetration of the flame, while effectively shielding the unexposed side of the foam from high temperature. During the test, the sample is gradually consumed by the impinging flame that eventually manages to pierce trough after an average of 90 s. The 6 BL 0.5M coating tremendously improves the foam resistance, by preserving the structure for more than 6 min (Figure 6b) and keeping the unexposed side temperature (plateau of 104 °C) well below the limit for its thermal degradation, (Figure 6c). This indicates a temperature drop from the exposed side of 850 °C with a temperature gradient greater than 500 °C cm^{-1}. These performances were compared with those of a silica aerogel that is notoriously known as an extremely efficient thermal insulating material. During the flame penetration tests, the aerogel shows the formation of small cracks on the surface directly exposed to the flame. A plateau of 102 °C on the unexposed side points out a temperature drop similar to the 6 BL 0.5M samples although this is achieved with thinner samples (1 vs 1.5 cm for aerogel and treated PU foams, respectively). However, it has to be noted that aerogels are also extremely brittle and rigid, unable to withstand even minimal mechanical deformations, while the LbL coated PU foams obtained in this work retain their high flexibility and elasticity as reported in Figure 6d and Videos S1 and S2 (Supporting Information). This comparison further highlights the impressive results achieved by our novel coated organic foam, possessing a set of physical properties that may outperforms conventional inorganic aerogels.

3. Conclusions

The present paper reported the preparation of self-extinguishing, nonignitable and flame resistant open cell polyurethane foams, via thin coating with a multilayered nano-exoskeleton comprising graphene oxide nanoplatelets deposited with a layer-by-layer approach. The inclusion of a phosphate salt within the LbL deposition has been proven to increase the thickness of the deposited coatings and confer additional flame retardant features to the coated foams. Only 3BL deposited at modified ionic strength are required to achieve self-extinguishing behavior during flammability tests and completely prevent ignition during cone calorimetry tests. These results outperform those of previously reported LbL assemblies on PU

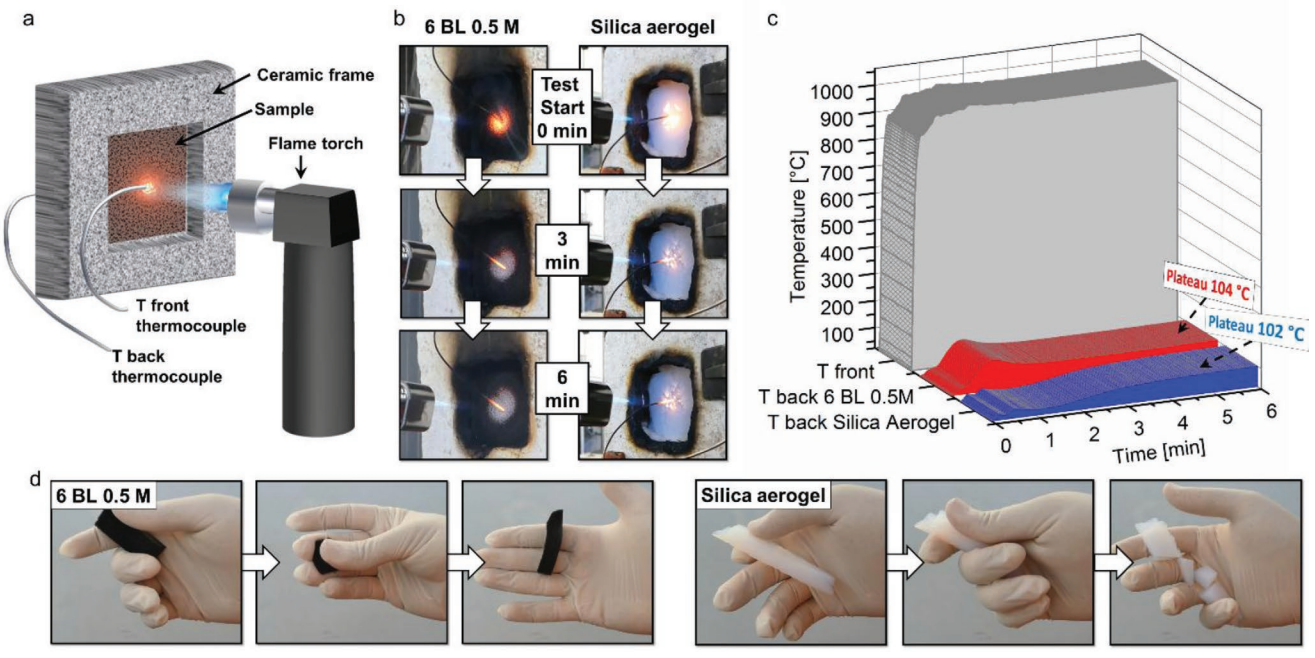

Figure 6. Flame penetration tests: a) schematic representation of the layout adopted for the test, b) digital pictures of the 6 BL 0.5M and silica aerogel front surface during the test, and c) front and back side temperatures as a function of time for 6 BL 0.5M and silica aerogel. d) simple bending test performed on 6 BL 0.5M foam and silica aerogel.

foams achieving a new standard in flame retardancy properties. Microstructural and chemical composition changes in the coated foams have been investigated highlighting the mechanism behind such impressive results. Mechanical reinforcement of the foam structure and the control over the release of flammable volatiles has been identified as the main flame retardant mechanisms controlling PU foam burning behavior.

In addition, foams coated by 6 BL at modified ionic strength have been found capable of withstanding the penetration of an impinging flame torch (T surface ≈950 °C), successfully insulating the unexposed side of the sample which temperature remained ≤100 °C for the whole duration of the test. These results proved these novel coated PU foams to be an efficient and sustainable alternative to the state of the art inorganic aerogels in terms of heat shielding. Furthermore, the excellent flexibility and toughness outperforms the inorganic aerogels, in all the application subject to mechanical deformations, vibration and impact.

In conclusion, the easy, sustainable, and industrially viable process proposed paves the way to the development of a new generation of materials based on graphene capable of greatly improving the fire safety of flexible foams employed in upholstered furniture and packaging (transports, buildings), soundproofing in buildings (theatres/cinemas, public rooms) and industrial applications (engine compartments, compressors, etc.).

4. Experimental Section

Materials: Commercially available PU foam with a density of 18 g dm^{-3} and thickness of 15 mm was purchased from a local warehouse. In order to remove dust an processing residues, PU foam samples were washed with deionized water and dried in oven at the temperature of 80 °C. PDAC (average M_w 400 000–500 000, 20 wt% in H_2O), polyacrylic acid (PAA, solution average M_w ≈100 000, 35 wt% in H_2O), branched poly(ethylene imine) (BPEI, M_w ≈25 000 by laser scattering, M_n ≈10 000 by gel permeation chromatography, as reported in the material datasheet) and APD were purchased from Sigma-Aldrich (Milano, Italy). GO were prepared by AVANZARE Innovacion Tecnologica (Navarrete -La Rioja, Spain) as 1 wt% suspension in water. The description of GO preparation is reported in the supporting information file and Figure S1 (Supporting Information) reports the Raman spectrum of prepared GO. 18.2 MΩ ultrapure water supplied by a Q20 Millipore system (Milano, Italy) was used for the preparation of the solutions and suspensions employed in this work. BPEI and PDAC solutions were employed at 0.1 wt% while PAA was diluted to 1 wt%. GO suspension was diluted to 0.5 wt%; APD 0.5 M was added to the GO suspension in order to modify ionic strength. All solutions and suspensions were kept under magnetic stirring at room temperature for at least 12 h.

Layer-by-Layer Deposition: Si wafer ((100), single side polished) was employed as model substrate in order to monitor the LbL growth by FT-IR spectroscopy. In order to prime the surface and prepare it for the LbL deposition, Si wafers were dipped for 10 min in the BPEI (positive charge) solution followed by 10 min in the PAA solution (negative charge). This pretreatment activates the substrate with a negative charge and mimic the procedure employed on PU foams. After this surface activation, the Si wafers were alternately dipped in the PDAC solution and GO suspension thus allowing for the alternate deposition of positively and negatively charged layers on the substrate.[11] The dipping time for the first adsorbed bilayer (i.e., one PDAC/GO pair) was set to 5 min; subsequent layers were obtained after 1 min. After each deposition step (including the first BPEI and PAA deposition), the Si wafer was washed by static dipping in ultrapure water for 1 min and then dried using dust- and oil-filtered compressed air. IR spectra were collected in transmission mode on dried samples after each deposition step, up to 10 BL. This procedure was employed to monitor the assembly of the PDAC/GO and PDAC/GO_0.5M_APD systems. Prewashed PU foams were first exposed to the PAA solution in order to activate the surface due to hydrogen bonding between the urethane groups and the undissociated carboxylic groups (the degree of dissociation of PAA in 1 wt% is averagely below 5%). Then, PU foams were alternatively dipped into the positive polyelectrolyte solution positively (PDAC) and the negatively charged nanoplatelets suspension (GO or GO_0.5M_APD) and washed with ultrapure water after each deposition. During each deposition and washing step the foams were vigorously squeezed several times in order to impregnate the foam complex structure with the employed solution/suspension or washing water. Dipping times were kept consistent with the ones employed for Si wafers. The process was repeated in order to deposit 3 or 6 BL. At the end of the LbL deposition, the treated foams were dried to constant weight in a ventilated oven at 80 °C. In the followings 3BL denotes a sample coated with 3BL of the PDAC/GO assembly while 3BL 0.5M denotes a sample coated with the PDAC/GO 0.5M APD assembly. The mass gain was evaluated by weighting the samples before and after the LbL deposition and is reported in Table S1 (Supporting Information).

Characterization: A FT-IR spectrometer (Perkin Elmer mod. Frontier, 32 scansions, 4 cm^{-1} resolution) was used to monitor the growth of the LbL assembly on model Si wafer surfaces following the procedure described above. The cross section of Si wafers and the surface morphology of untreated and LbL-treated PU foams were evaluated by FESEM (Zeiss Merlin 4248, beam voltage: 5 kV). Si wafer were simply broken by mechanical stress (bending) in order to obtain the coating cross section as a consequence of the Si fragile fracture. PU foams were cut into small pieces (≈10 × 10 × 5 mm^3). Samples were pinned up on conductive adhesive tapes and chromium coated prior to FESEM observations.

The morphology and chemical composition of post combustion residues was investigated using a LEO-1450VP Scanning Electron Microscope equipped with a X-ray probe (INCA Energy Oxford, Cu Kα X-ray source, k = 1.540562 Å). Beam voltage was set to 5 kV for imaging and to 20 kV for elemental analyses. The samples positioned on conductive tape were gold coated prior to observation. Flammability tests were performed in horizontal configuration by applying a 20 mm blue methane flame on the short side of specimen (50 × 150 × 15 mm^3) positioned on a metallic grid, accordingly with ASTM D 4986 standard. The flame was first applied for 3 s; when self-extinguishment occurred a second flame application of 6 s was performed. The test was repeated on 3 different samples for each coating composition. During the test the formation of incandescent droplets of molten polymer (melt dripping) was evaluated by placing dry cotton underneath the sample. The final residue was evaluated by weighting the sample before and after the test. Cone calorimetry (Fire Testing Technology,) was employed to investigate the combustion behavior of 50 × 50 × 15 mm^3 specimens under 35 kW m^{-2} radiative heat flux. Measurements were performed four times for each formulation evaluating time to ignition (TTI), peak of heat release rate (pkHRR), total heat release (THR), total smoke release (TSR,) and final residue. Average values are presented with their experimental deviations. Prior to flammability and cone calorimetry tests, all specimens were conditioned at 23 ± 1 °C for 48 h at 50% R.H. in a climatic chamber. Flame penetration test was performed in order to assess the resistance of coated samples to penetration of a 150 W flame generated from a butane flame torch. The test was carried out by placing square specimens (50 × 50 × 15 mm^3) in a ceramic frame, held in vertical configuration, and applying the flame toward the specimen center. The torch, positioned at 50 mm distance from the surface of the specimen, was applied continuously for 5 min. The temperature profiles on the front side surface (exposed to the flame) and on the back side of the specimen were measured by two thermocouples (stainless steel sheathed K-type; 1 mm diameter). The thermocouples were placed into contact with the sample and fixed ensuring that no displacement occurs during the test. The test was duplicated for each different

formulation. FT-IR ATR were collected at room temperature in the range 4000–700 cm^{-1} (16 scans and 4 cm^{-1} resolution) using a spectrometer (Perkin Elmer mod. Frontier) equipped with a germanium crystal. Raman spectra were performed on a InVia Raman Microscope (Renishaw, argon laser source 514 nm/50 mW, 10 scans) coupled with a Leica DM 2500 optical microscope. D and G bands were fitted with Gaussian_Lorentz Cross functions in order to determine their ratio.

Supporting Information

Supporting Information is available from the Wiley Online Library or from the author.

Acknowledgements

The EU H2020 project Graphene Flagship-Core 1 (grant agreement no. 696656) is acknowledged for financial support. Mr. Mauro Raimondo and Mr. Fabio Cuttica are acknowledged for FE-SEM analyses and cone calorimetry tests, respectively. In addition, the authors thank Dr. Samuele Colonna for the help and valuable discussions. F.C. and A.F. conceived the experiments, F.C. coordinated the project, F.C. and L.M. carried the LbL deposition and the characterization. J.G. provided the GO suspension and contributed to the discussion. A.F. contributed to the interpretation of results and G.S. participated to the discussion of the results. The manuscript was mainly written by F.C. and A.F.

Conflict of Interest

The authors declare no conflict of interest.

Keywords

flame retardancy, flexible foams, graphene oxide, layer-by-layer, thermal shielding

Received: August 21, 2018
Revised: September 7, 2018
Published online: October 8, 2018

[1] M. Ahrens, *Home Fires That Began with Upholstered Furniture*, National Fire Protection Association Quincy, MA, USA **2008**.
[2] J. Alongi, F. Carosio, *Novel Fire Retardant Polymers and Composite Materials*, Woodhead Publishing, Sawston, Cambridge, UK **2017**, p. 171.
[3] H. M. Stapleton, S. Klosterhaus, A. Keller, P. L. Ferguson, S. van Bergen, E. Cooper, T. F. Webster, A. Blum, *Environ. Sci. Technol.* **2011**, *45*, 5323.
[4] G. Stieger, M. Scheringer, C. A. Ng, K. Hungerbuhler, *Chemosphere* **2014**, *116*, 118.
[5] J. H. Troitzsch, *J. Fire Sci.* **2016**, *34*, 171.
[6] H.-B. Chen, D. A. Schiraldi, *Polym. Rev.* **2018**, *1*, 1.
[7] Y.-T. Wang, H.-B. Zhao, K. Degracia, L.-X. Han, H. Sun, M. Sun, Y.-Z. Wang, D. A. Schiraldi, *ACS Appl. Mater. Interfaces* **2017**, *9*, 42258.
[8] K. Shang, J.-C. Yang, Z.-J. Cao, W. Liao, Y.-Z. Wang, D. A. Schiraldi, *ACS Appl. Mater. Interfaces* **2017**, *9*, 22985.
[9] H. Sun, D. A. Schiraldi, D. Chen, D. Wang, M. Sánchez-Soto, *ACS Appl. Mater. Interfaces* **2016**, *8*, 13051.
[10] M. Ghanadpour, B. Wicklein, F. Carosio, L. Wågberg, *Nanoscale* **2018**, *10*, 4085.
[11] *Multilayer Thin Films: Sequential Assembly of Nanocomposite Materials*, 2nd ed., Wiley-VCH, Weinheim, Germany **2012**.
[12] K. M. Holder, R. J. Smith, J. C. Grunlan, *J. Mater. Sci.* **2017**, *52*, 12923.
[13] O. Koklukaya, F. Carosio, L. Wågberg, *ACS Appl. Mater. Interfaces* **2017**, *9*, 29082.
[14] J. Lefebvre, B. Bastin, M. Le Bras, S. Duquesne, C. Ritter, R. Paleja, F. Poutch, *Polym. Test.* **2004**, *23*, 281.
[15] Y. S. Kim, R. Davis, A. A. Cain, J. C. Grunlan, *Polymer* **2011**, *52*, 2847.
[16] D. Patra, P. Vangal, A. A. Cain, C. Cho, O. Regev, J. C. Grunlan, *ACS Appl. Mater. Interfaces* **2014**, *6*, 16903.
[17] G. Decher, *Science* **1997**, *277*, 1232.
[18] A. A. Cain, M. G. B. Plummer, S. E. Murray, L. Bolling, O. Regev, J. C. Grunlan, *J. Mater. Chem. A* **2014**, *2*, 17609.
[19] K. Apaydin, A. Laachachi, V. Ball, M. Jimenez, S. Bourbigot, D. Ruch, *Colloids Surf., A* **2015**, *469*, 1.
[20] K. Apaydin, A. Laachachi, V. Ball, M. Jimenez, S. Bourbigot, V. Toniazzo, D. Ruch, *Polym. Degrad. Stab.* **2013**, *98*, 627.
[21] F. Carosio, C. Negrell-Guirao, A. Di Blasio, J. Alongi, G. David, G. Camino, *Carbohydr. Polym.* **2015**, *115*, 752.
[22] F. Carosio, A. Di Pierro, J. Alongi, A. Fina, G. Saracco, *J. Colloid Interface Sci.* **2018**, *510*, 142.
[23] R. J. Smith, K. M. Holder, S. Ruiz, W. Hahn, Y. Song, Y. M. Lvov, J. C. Grunlan, *Adv. Funct. Mater.* **2017**, *28*, 1703289.
[24] F. Carosio, A. Di Blasio, F. Cuttica, J. Alongi, G. Malucelli, *RSC Adv.* **2014**, *4*, 16674.
[25] M. J. Nine, M. Ayub, A. C. Zander, D. N. Tran, B. S. Cazzolato, D. Losic, *Adv. Funct. Mater.* **2017**, *27*, 1703820.
[26] L. Dong, C. Hu, L. Song, X. Huang, N. Chen, L. Qu, *Adv. Funct. Mater.* **2016**, *26*, 1470.
[27] B. Dittrich, K.-A. Wartig, D. Hofmann, R. Mülhaupt, B. Schartel, *Polym. Degrad. Stab.* **2013**, *98*, 1495.
[28] B. Wen, M. Cao, M. Lu, W. Cao, H. Shi, J. Liu, X. Wang, H. Jin, X. Fang, W. Wang, J. Yuan, *Adv. Mater.* **2014**, *26*, 3484.
[29] M. Cao, X. Wang, W. Cao, X. Fang, B. Wen, J. Yuan, *Small* **2018**, *14*, 1800987.
[30] X. Zhang, Q. Shen, X. Zhang, H. Pan, Y. Lu, *J. Mater. Sci.* **2016**, *51*, 10361.
[31] B. Wicklein, A. Kocjan, G. Salazar-Alvarez, F. Carosio, G. Camino, M. Antonietti, L. Bergström, *Nat. Nanotechnol.* **2015**, *10*, 277.
[32] L. Maddalena, F. Carosio, J. Gomez, G. Saracco, A. Fina, *Polym. Degrad. Stab.* **2018**, *152*, 1.
[33] W. Sun, W.-l. Liu, Y.-h. Hu, *J. Central South Univ. Technol.* **2008**, *15*, 373.
[34] Y. Si, E. T. Samulski, *Nano Lett.* **2008**, *8*, 1679.
[35] G. Socrates, *Infrared and Raman Characteristic Group Frequencies—Table and Charts*, Wiley, Chichester, UK **2006**.
[36] A. F. Xie, S. Granick, *Macromolecules* **2002**, *35*, 1805.
[37] E. Kharlampieva, S. A. Sukhishvili, *Langmuir* **2003**, *19*, 1235.
[38] K. Krogman, N. Zacharia, S. Schroeder, P. Hammond, *Langmuir* **2007**, *23*, 3137.
[39] F. Carosio, J. Alongi, *ACS Appl. Mater. Interfaces* **2016**, *8*, 6315.
[40] F. Carosio, C. Negrell-Guirao, J. Alongi, G. David, G. Camino, *Eur. Polym. J.* **2015**, *70*, 94.
[41] X. Mu, B. Yuan, Y. Pan, X. Feng, L. Duan, R. Zong, Y. Hu, *Mater. Chem. Phys.* **2017**, *191*, 52.
[42] X. Wang, Y.-T. Pan, J.-T. Wan, D.-Y. Wang, *RSC Adv.* **2014**, *4*, 46164.
[43] M. Haile, S. Fomete, I. D. Lopez, J. C. Grunlan, *J. Mater. Sci.* **2016**, *51*, 375.
[44] K. M. Holder, A. A. Cain, M. G. Plummer, B. E. Stevens, P. K. Odenborg, A. B. Morgan, J. C. Grunlan, *Macromol. Mater. Eng.* **2016**, *301*, 665.
[45] G. Laufer, C. Kirkland, A. A. Cain, J. C. Grunlan, *ACS Appl. Mater. Interfaces* **2012**, *4*, 1643.
[46] A. C. Ferrari, D. M. Basko, *Nat. Nanotechnol.* **2013**, *8*, 235.
[47] S. Claramunt, A. Varea, D. López-Díaz, M. M. Velázquez, A. Cornet, A. Cirera, *J. Phys. Chem. C* **2015**, *119*, 10123.
[48] B. Yu, Y. Shi, B. Yuan, S. Qiu, W. Xing, W. Hu, L. Song, S. Lo, Y. Hu, *J. Mater. Chem. A* **2015**, *3*, 8034.
[49] K. Kishore, K. Mohandas, *Combust. Flame* **1981**, *43*, 145.